Long-Range Nature of the Interactions between Titratable Groups in *Bacillus agaradhaerens* Family 11 Xylanase: pH Titration of *B. agaradhaerens* Xylanase[†]

Marco Betz, Frank Löhr, Hans Wienk,[‡] and Heinz Rüterjans*

Institute of Biophysical Chemistry, Center for Biomolecular Magnetic Resonance, Johann Wolfgang Goethe-University, Biocentre N230, Marie Curie-Strasse 9, D-60439 Frankfurt am Main, Germany

Received January 7, 2004; Revised Manuscript Received March 12, 2004

ABSTRACT: Xylanase from *Bacillus agaradhaerens* belongs to a large group of glycosyl hydrolases which catalyze the degradation of xylan. The protonation behavior of titratable groups of the uniformly ^{15}N- and ^{13}C-labeled xylanase was investigated by multinuclear NMR spectroscopy. A total of 224 chemical shift titration curves corresponding to ^{1}H, ^{13}C, and ^{15}N resonances revealed pK_a values for all aspartic and glutamic acid residues, as well as for the C-terminal carboxylate and histidine residues. Most of the titratable groups exhibit a complex titration behavior, which is most likely due to the mutual interactions with other neighboring groups or due to an unusual local microenvironment. Subsite −1 containing the catalytic dyad shows a long-range interaction over 9 Å with Asp21 via two hydrogen bonds with Asn45 as the mediator. This result illuminates the pivotal role of the conserved position 45 among family 11 endoxylanases, determining an alkaline pH optimum by asparagine residues or an acidic pH optimum by an aspartate. The asymmetric interactions of neighboring tryptophan side chains with respect to the catalytic dyad can be comprehended as a result of hydrogen bonding and aromatic stacking. Most of the chemical shift−pH profiles of the backbone amides exhibit biphasic behavior with two distinct inflection points, which correspond to the pK_a values of the nearby acidic side chains. However, the alternation of both positive and negative slopes of individual amide titration curves is interpreted as a consequence of a simultaneous reorganization of side chain conformational space at pH ≈6 and/or an overall change in the hydrogen network in the substrate binding cleft.

Structure and function of many proteins are intimately dependent on the protonation equilibria of ionizable groups. Most enzymes perform catalysis with the assistance of ionizable groups that act either as a Brønsted acid or base, as ligands, or less directly through the generated electrostatic potential at the active site (*1*). Buried ionizable residues can make favorable or unfavorable contributions to protein stability (*2*). Many such groups exhibit perturbed pK_a values whose shifts are discussed with a variety of possible interactions (*3*−*5*). Charge−charge and charge−dipolar interactions between amino acid side chains contribute to the energetics of protein folding together with hydrogen bonds and hydrophobic interactions. In recent years, structure-based calculations of electrostatic energy and pK_a values have been the subject of many theoretical investigations, which contribute to our understanding of the physical character and structural origins of electrostatic effects (*6*−*9*). Though computer technology has advanced during the past several years, allowing sophisticated algorithms to work at a moderate time scale, the precision and accuracy of predicted electrostatic energies and pK_a values remain challenging. Because of the complex theory of protein electrostatics, numeric calculations rely on simplifying assumptions regarding issues such as the charge distribution within the protein, the polarizability of this distribution, and rating the protein and its surrounding solvent as a homogeneous or heterogeneous medium. One of the major problems arises from the difficulties in capturing quantitatively the dielectric properties of the protein at a given structure(s). The implicit use of dielectric constants must still be calibrated against experimental data in each model system (*10*), thus renewing the interest for experimental characterization of electrostatic effects in proteins.

In this study, the complex, long-range nature of interactions between titratable groups in *Bacillus agaradhaerens* family 11 xylanase (BadX)[1] was investigated. The enzyme with a molecular mass of 23 kDa carries out xylan hydrolysis via a two-step mechanism involving a covalent enzyme−glycosyl intermediate (*11*). Initially, the carboxylate of

[†] Supported by a grant from the Alexander-von-Humboldt Foundation.

* To whom correspondence should be addressed. Telephone: +49-69-79829630. Fax: +49-69-79829632. E-mail: hruet@bpc.uni-frankfurt.de.

[‡] Present address: Department of of NMR Spectroscopy, University of Utrecht, Bijvoet Center for Biomolecular Research, Padualaan 8, 3584 CH Utrecht, The Netherlands.

[1] Abbreviations: BadX, *B. agaradhaerens* xylanase; BCX, *B. circulans* xylanase; Δδ, difference in chemical shifts upon titration from high to low pH; δ_a, chemical shift of the Brønsted acid; δ_b, chemical shift of the corresponding Brønsted base; DSS, 2,2-dimethyl-2-silapentane-5-sulfonate; HSQC, heteronuclear single-quantum coherence; N35D, substitution of asparagine for aspartic acid 35; NMR, nuclear magnetic resonance; SDS−PAGE, sodium dodecyl sulfate−polyacrylamide gel electrophoresis; TROSY, transverse relaxation-optimized spectroscopy; XYNII, *T. reesei* xylanase II.

10.1021/bi049948m CCC: $27.50
Published on Web 04/22/2004

Glu184 functions as a Brønsted acid, protonating the glycosidic bond to assist leaving group departure. Glu94 performs a nucleophilic attack at the substrate anomeric center, forming an intermediate bond. In the second step, hydrolysis proceeds in the reverse order with water as the nucleophilic agent and Glu184 functioning as a Brønsted base. BadX adopts the same overall fold and topology as the other family 11 xylanase structures (*12*−*14*): a single-domain polypeptide chain containing two β-sheets, A and B, composed of five and eight β-strands, respectively. The two antiparallel β-sheets are twisted around a deep, long cleft, which is lined with many aromatic and acidic residues. It is large enough to accommodate at least four xylose moieties, whose corresponding binding subsites are labeled from −3, −2, −1, to 1 with cleavage taking place between the −1 and +1 subsites (*15*). The loop between strands A7 and A8 forms the "thumb", which is perpendicular above the substrate binding cleft, and the overall structure resembles a partially closed right hand (*16*).

Generally, the paper and pulp industry makes use of the specificity of the xylan degradation because pretreatment of paper pulp with xylanases enhances the bleaching process. Smaller amounts of bleaching chemicals are required, thereby reducing environmentally toxic byproducts and economic costs. As shown previously (*17*), BadX has enhanced stability under conditions of elevated pH and temperature, which is a quality already utilized in industrial scale (*18*). Because of this stability, BadX was chosen as an appropriate model for the determination of pH-dependent chemical shift values by multinuclear NMR spectroscopy. Titration curves obtained from the pH-dependent ^{13}C and ^{15}N chemical shifts are analyzed by nonlinear least-squares fitting to simple relationships derived from the Henderson−Hasselbach equation. On the basis of the crystal structure (*11*), the relationship between observed pK_a values and the corresponding microenvironment is discussed to provide a comprehensive evaluation of electrostatic interactions. For this approach, the sensitivity of chemical shifts of amide groups to changes in the local environment is utilized. It is well-known that chemical shifts of amide groups are very sensitive to backbone conformation and to the electrical charge field generated by ions, weaker multipoles in their vicinity. Hydrogen bonding is also very important for the values of shielding, and torsion angles of side chains may also have a less significant effect (*19*, *20*). As consequence, the resonances of the inspected reporter amides can be influenced not only by changes in the electrostatic field but also by changes in the arrangement of hydrogen bond network or side chain conformations.

EXPERIMENTAL PROCEDURES

Sample Preparation. Uniformly doubly ^{15}N- and ^{13}C-labeled recombinant BadX (residues 1−207) was expressed in *Escherichia coli* expression strain BL21(DE3) using a pET-3a-BadX plasmid construct. The protein was purified as previously described (*21*) with the following modification. The purified protein was rebuffered in 10 mM d_3-NaOAc (pH 5.3) with a 90% H_2O/5% D_2O/5% d_5-glycerol mixture containing 50 mM $MgCl_2$. Sample concentrations were kept below 0.5 mM because of a tendency for the samples to precipitate reversibly at higher concentrations within the range of pH 6−9. The concentration of the protein sample was quantified by UV absorbance measurement at 280 nm using a calculated extinction coefficient (ϵ_{280}) of 56.47 mM^{-1} cm^{-1} (*22*), and the purity (>99%) was assessed by discontinuous SDS−PAGE. The protein samples used for the titration were initially at pH 5.3, and the pH was lowered or raised by the appropriate addition of small aliquots of 1 M HCl or NaOH. The pH was measured before and after acquisition of the set of NMR experiments for each titration point at 303 K, and the average of the initial and final value was recorded. The reported values were not corrected for the deuterium isotope effect, and the uncertainty was assumed to be 0.05 pH unit. To verify the reversibility of the pH titration, the acidic sample was adjusted step by step back to pH 5.7 while the same set of NMR experiments was repeated.

NMR Measurements. Chemical shifts of backbone amide and tryptophan indole $N^{\epsilon 1}$ resonances were followed during pH titration via two-dimensional $^{15}N-^{1}H$ -TROSY-HSQC (*23*). The experiments were recorded with 1024 (F_2) × 256 (F_1) complex points with spectral widths of 9713 (F_2) and 3041 Hz (F_1) and acquisition times of 127 ms. The behavior of the carboxyl and carboxamide side carbons of Asx and Glx as a function of pH was monitored using a two-dimensional version of the H(CA)CO experiment (*24*, *25*), modified to optimize the detection of the $H^{\beta}(C^{\beta})C^{\gamma}$ and H^{γ}-$(C^{\gamma})C^{\delta}$ correlations of all Asx and Glx residues, respectively (*26*). The spectral widths were 6003 and 2392 Hz in F_2 and F_1, respectively, with 512 (F_2) × 256 (F_1) complex points and acquisition times of 102 ms. A two-dimensional $H^{\delta 2}C^{\delta 2}C^{\gamma}$/$H^{\epsilon 1}C^{\epsilon 1}$ correlation experiment, abbreviated as CT-HCDCG^{His} (*3*), was used to investigate the pH dependence of chemical shifts of histidine residues. The spectra were acquired with 384 (F_2) × 98 (F_1) complex points with spectral widths of 5685 (F_2) and 3787 Hz (F_1) and acquisition times of 81 ms. All experiments were carried out at 303 K on a Bruker DMX 500 spectrometer equipped with a 5 mm three-axis gradient $^{1}H\{^{13}C^{15}N\}$ triple-resonance probe. ^{1}H resonance positions were calibrated with an internal 2,2-dimethyl-2-silapentane-5-sulfonate (DSS) standard, while indirect referencing according to the absolute frequency values was used for ^{13}C and ^{15}N chemical shifts (*27*). The data were processed using XWINNMR version 2.1 (Bruker Biospin, Rheinstetten, Germany) and analyzed with NMRVIEW version 5.0.4 (Merck and Co. Inc., Rahway, NJ). In general, π/2-shifted squared sine apodization functions were applied prior to Fourier transformation. Appropriate zero filling led to a digital resolution of typically 4.0−6.1, 4.7−4.9, and 4.9 Hz/point in the ^{1}H, ^{13}C, and ^{15}N dimensions, respectively.

pH-Dependent Chemical Shift Data Analysis. Cross-peaks were assigned in the set of spectra at pH 5.3 by reference to the reported chemical shift assignments at that pH (*21*). pH-dependent chemical shifts were then followed incrementally to pH 3.2 and 8.7, respectively. The estimated uncertainties of the chemical shifts used in the data analysis are 0.02 and 0.1 ppm for ^{1}H and heteronuclei, respectively. The pH dependence of the chemical shift observed for an appropriate reporter nucleus was fitted by modified Henderson−Hasselbach equations describing up to three protonation and/or deprotonation processes, which were assumed to be independent in all cases (*28*, *29*):

$$\delta(\mathrm{pH}) = \delta_b + \sum_{i=1}^{j} \frac{c_i(\delta_a - \delta_b) \times 10^{pK_{ai}-pH}}{1 + 10^{pK_{ai}-pH}}; \sum_{i=1}^{j} c_i = 1; \quad j = 1, 2, \text{or } 3$$

where δ(pH) is the observed chemical shift for the resonance of the reporter nucleus at a given pH and δ_a and δ_b denote the limiting chemical shifts of this resonance at acidic and basic pH, respectively. pK_{ai} is the negative common logarithm of the apparent acid dissociation constant for the *i*th protonation or deprotonation process reflected by the reporter resonance. In the case of analyzed backbone amide and tryptophan indole $N^{\epsilon 1}$ resonances, pK_{ai} describes the *i*th inflection point correlating to a nearby titration event. The product $c_i(\delta_a - \delta_b)$ represents the contribution of this protonation or deprotonation step to the total chemical shift change ($\delta_a - \delta_b$). pK_{ai} values and additional parameters (c_i or δ_a, δ_b) were determined from the experimental data by the Levenberg−Marquardt or the Simplex nonlinear least-squares fitting procedure using Origin version 6.0 (Microcal Software Inc., Northampton, MA). Reported errors relate to the precision of the data fitting, but not to the uncertainties of the data acquisition or resonance assignment.

The choice of the number of *j* protonation or deprotonation processes required to fit the experimental data to the modified Henderson−Hasselbach equation was made mainly by *F*-test statistics (*30*) using a confidence level of 99%. Also, structural considerations were taken into account in a reliable determination of the number (*j*) of protonation or deprotonation steps. For this, measurements of the distance from reporter atoms to nearby ionizing atoms were carried out for the crystal structure of free BadX (Protein Data Bank entry 1QH7).

RESULTS

pH Dependence of Backbone ^{15}N Resonances. Detailed electrostatic properties of the protein can be obtained by using all backbone amide nitrogen resonances as probes, which are distributed all over the protein globule. For this approach, all pH-dependent backbone amide resonances were assigned for the 24 $^{15}N-^{1}H$ TROSY-HSQC spectra, and additionally, the seven indole side chain resonances were analyzed. All chemical shift values were standardized in both dimensions by the equation $\delta(H^N,N_{bb}) = \sqrt{(\delta^2_H + \delta^2_N \times 0.16^2)}$ (*31*, *32*), and the difference between the minimal and maximal pH-dependent chemical shift values for a given residue was calculated. A total chemical shift change ($\delta_{max} - \delta_{min}$) of <0.1 ppm was considered to be insignificant due to the estimated uncertainties of data analysis. The changes in chemical shift values were arbitrarily divided into five groups, and relative colors were assigned (Figure 1). This color index was projected on the structure of the enzyme (Figure 2) to illustrate which backbone amides are strongly perturbed upon pH titration or which amides are independent.

Figure 2A shows that the large cleft, which is created by the highly twisted interior β-sheet, is ideally suited to serving as a substrate binding pocket. It is lined with the majority of the aspartate and glutamate residues, including the two conserved residues which are involved in catalysis, Glu94 and Glu184. This is the reason the backbone amides of the interior β-sheet are more perturbed upon pH titration than

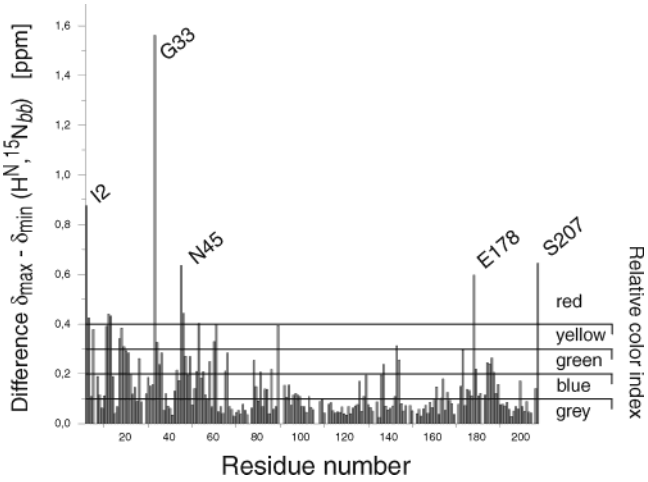

FIGURE 1: Chemical shift perturbations of backbone amides observed upon pH titration. ^{1}H and ^{15}N dimensions were standardized as described in the text, and the differences [$\delta_{max} - \delta_{min}$ (H^N, N_{bb})] were calculated. Gradation into relative colors for Figure 2: residues with chemical shift perturbations of <0.1 ppm considered insignificantly (gray), <0.2 ppm weakly (blue), <0.3 ppm intermediately (green), <0.4 ppm strongly (yellow), and >0.4 ppm very strongly (red) perturbed.

the second β-sheet. The chemical shift values belonging to the residues at the convex outside (Figure 2B) remain unaffected by the influences of pH titration. This outside is mostly built by the outer five-stranded β-sheet, which lacks any titratable side chains. Close to this β-sheet is located the hydrophobic core of the enzyme, which is bordered by amphiphatic α-helix 2 and the opposite side of the inner β-sheet. His162 is buried within this core of three neighboring acidic side chains, Asp99, Asp118, and Asp123. Neither the amides of the protein backbone nor the four titratable side chains show any significant changes in chemical shift values during the course of pH titration.

Protonation Behavior of Side Chain Carboxyl Groups in BadX. Modified two-dimensional H(CA)CO experiments were performed from pH 3.2 to 8.7 to probe the titration behavior of BadX aspartate and glutamate groups. All eight aspartic and six of seven glutamic amino acid residues present in BadX could be unambiguously identified in the set of incremental NMR spectra. The pH dependence of the chemical shifts of the side chain carboxyl carbon resonances is presented in panels A and B of Figure 3. Only the side chain carboxyl resonances of Asp5, Asp90, Glu56, and Glu126 exhibited essentially monophasic titration behavior, which is well-known from model compounds (*33*, *34*). All the other acidic side chains exhibited minor inflections on the titration curves due to the nearby ionizable groups. The corresponding pK_a values derived from fitting titration curves with up to three pK_a values to the titration data are summarized in Table 1. When more than one pK_a value was required for a reasonable fit, the residues assumed to contribute to this titration behavior are listed.

For protonated aspartic acid and glutamic acid, the carboxyl carbons resonate between 177.5 and 181.3 and between 177.8 and 183.5 ppm, respectively, while the signals from the ionized forms are ~0.5−3.5 ppm downfield. However, the C^{γ} resonance of Asp21 experiences a distinct reverse shift at higher pH values. In comparison to average values, the $C^{\gamma/\delta}$ resonances of Asp15 and Glu167 are

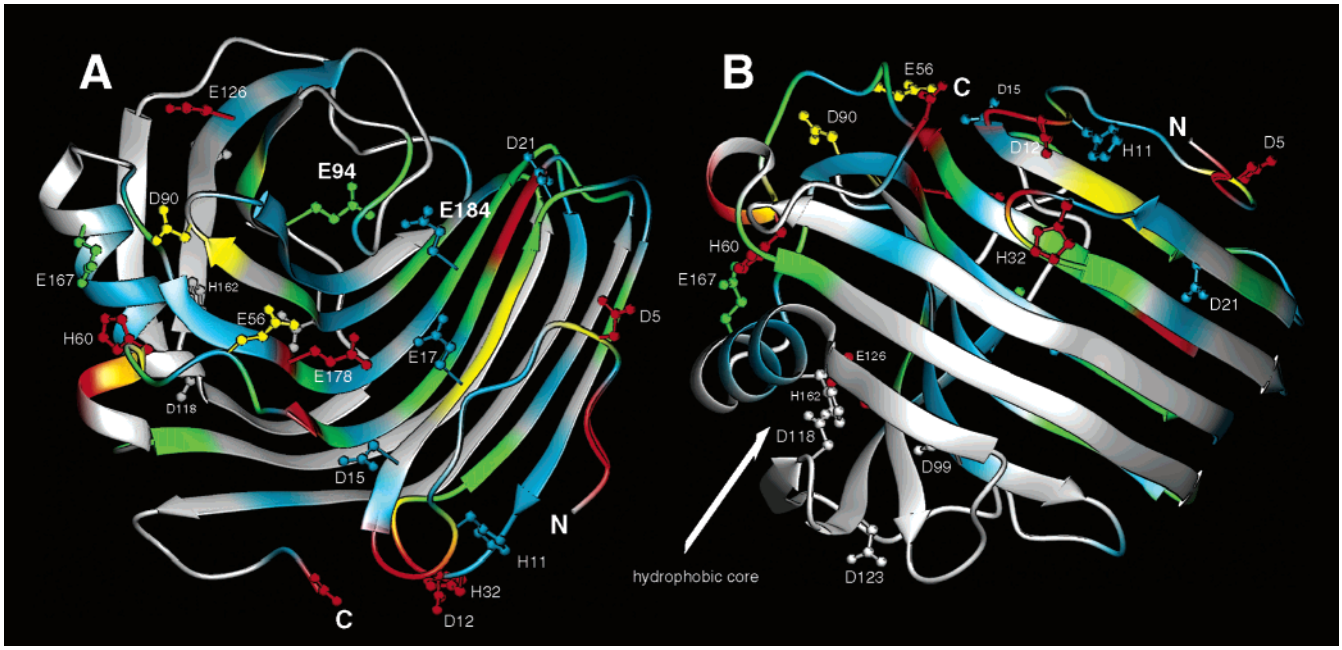

FIGURE 2: Structure of recombinant BadX colored due to the relative color index as described in the text, which is based on chemial shift perturbations observed upon pH titration. The differences ($\delta_{max} - \delta_{min}$) between the minimal and maximal pH-dependent chemical shift values for backbone $^{1}H^{N}$ and $^{15}N_{bb}$ amides, $^{13}C^{\gamma/\delta}$ carboxyl groups, and histidine side chain $^{13}C^{\gamma/\delta2/\epsilon1}$ groups were considered. (A) Side view and (B) bottom view: (gray) insignificant chemical shift perturbations, (blue) weak perturbations, (green) intermediate perturbations, (yellow) strong perturbations, and (red) very strong perturbations. The ribbon drawing was created with MOLMOL (*53*).

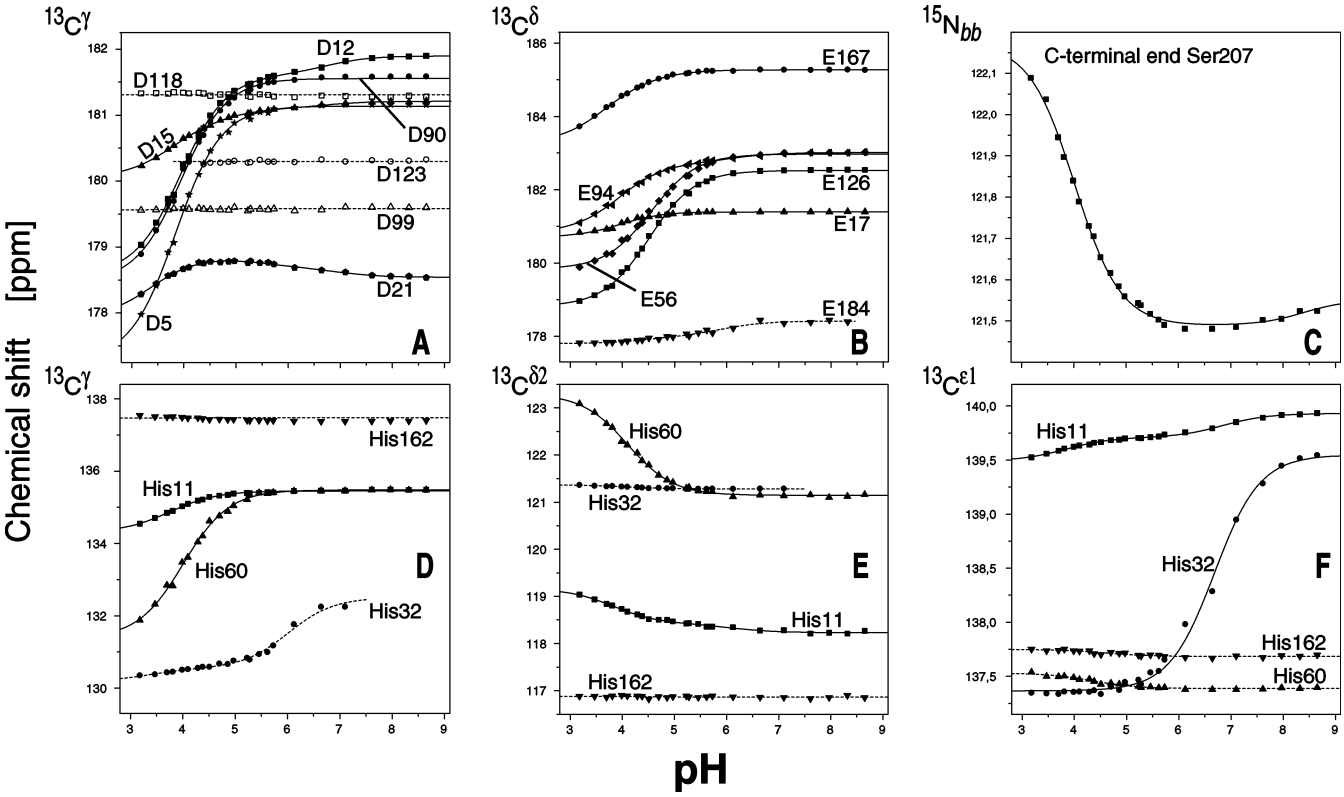

FIGURE 3: pH-dependent chemical shift values for titratable groups in recombinant BadX. Experimental titration curves as determined by $^{1}H-^{13}C$ and $^{1}H-^{15}N$ correlation NMR spectroscopy in the pH range of 3.2−8.7. Symbols are experimental data points, and lines represent nonlinear least-squares fits to modified Henderson−Hasselbach equations according to the noninteracting model with one [$j = 1$; D5 (★), D90 (●), E17 (▲), E56 (◆), E126 (■), His32 $C^{\epsilon1}$ (●), and His60 $C^{\gamma,\delta2}$ (▲)], two [$j = 2$; D12 (■), E94 (triangle pointing to the left), E167 (●), His11 $C^{\gamma,\delta2,\epsilon1}$ (■), and Ser207 COOH (■)], or three [$j = 3$; D15 (▲) and D21 (⬟)] apparent pK_a values. Dashed lines show the uncertainty in the determination of the proper pK_a value: D99 (△), D118 (□), D123 (○), E184 (▼), His32 $C^{\gamma,\delta2}$ (●), His60 $C^{\epsilon1}$ (▲), and His162 $C\gamma^{\delta2,\epsilon1}$ (▼).

unusually shifted downfield, whereas the C^{δ} resonances of Glu184 and the $H^{\gamma/\gamma'}$ resonances of Glu94 are shifted upfield. The chemical shifts of residues Asp15, Asp21, Glu17, Glu167, and Glu184 undergo a substantially smaller pH

Table 1: pK_a Values[a] of BadX Titratable Groups Measured by NMR in H_2O at 303 K in the pH Range 3.2−8.7

residue	reporter nucleus	pK_a value	$\Delta\delta$[b] (ppm)	accessibility[c] to solvent (%)	additional titration event[d] and/or tautomeric state
Asp5	C^γ	3.84 ± 0.02	3.85	42.6	
Asp12	C^γ	3.94 ± 0.14	3.31	42.5	His11/His32 (6.73 ± 0.16, $c_2 = 0.08$)
Asp15	C^γ	3.35 ± 0.14	1.41	15.6	Glu17 (4.47 ± 0.13, $c_2 = 0.28$) (6.66 ± 0.14, $c_3 = 0.08$)
Asp21	C^γ	3.46 ± 0.13	0.51	25.5	Glu184 via Asn45 (5.3 ± 0.3, $c_2 = -0.31$; 6.9 ± 0.3, $c_3 = -0.33$)
Asp90	C^γ	3.88 ± 0.07	3.08	58.5	
Asp99, Asp118, Asp123	C^γ	<2.7[e]	<0.08	1.3, 20.4, 6.8	
Glu17	C^δ	4.31 ± 0.07	0.71	9.2	
Glu56	C^δ	4.55 ± 0.02	3.14	25.6	
Glu94	C^δ	3.94 ± 0.04	2.18	7.2	Glu184 (6.14 ± 0.21, $c_2 = 0.13$)
Glu126	C^δ	4.51 ± 0.02	3.71	22.1	
Glu167	C^δ	3.58 ± 0.13	2.04	26.8	His60 (4.41 ± 0.28, $c_2 = 0.19$)
Glu178	N_{bb} amides	4.1 ± 0.2		2.4	
Glu184	N_{bb} amides	6.5 ± 0.2		3.3	
	C^δ	–[f]	0.62		Glu94 (4.39 ± 0.52, $c_1 = 0.29$)
C-terminus	H^N u. N_{bb}	3.9 ± 0.1		64.7	
His11	C^γ	6.52 ± 0.26	1.20	19.2	Asp12 (3.71 ± 0.02, $c_1 = 0.95$); $N^{\epsilon 2}$−H tautomer
	$C^{\delta 2}$	6.09 ± 0.18	0.93		Asp12 (3.82 ± 0.07, $c_1 = 0.80$)
	$C^{\epsilon 1}$	6.84 ± 0.05	0.44		Asp12 (3.85 ± 0.06, $c_1 = 0.49$)
His32	C^γ	–[f]	2.00	48.5	Asp12 (3.36 ± 0.84, $c_1 = 0.15$)
	$C^{\delta 2}$	–[f]	0.09		
	$C^{\epsilon 1}$	6.68 ± 0.03	2.18		$N^{\epsilon 2}$−H tautomer for pH <7.1; equilibrium between both tautomers at pH >7.1
His60	C^γ	4.01 ± 0.02	4.09	4.7	$N^{\epsilon 2}$−H tautomer
	$C^{\delta 2}$	4.11 ± 0.02	2.15		
	$C^{\epsilon 1}$	–[f]	0.14		
His162	C^γ	<2.7[e]	<0.08	0.7	no titration event; $N^{\epsilon 2}$−H tautomer
	$C^{\delta 2}$	<2.7	<0.08		
	$C^{\epsilon 1}$	<2.7	<0.06		

[a] Apparent pK_a values of ionizable groups were determined by analysis of experimental data obtained by NMR spectroscopy. Nonlinear least-squares fittings to a modified Henderson−Hasselbach equation according to the noninteracting model were performed as described in the text. [b] $\Delta\delta$ ($\delta_b - \delta_a$) denotes the difference in the limiting chemical shifts of the protonated and deprotonated forms, obtained as part of the fitting procedure. [c] The solvent-accessible surface was estimated for the whole residue using MOLMOL (*53*) and a probe size of 1.4 Å. [d] Residues assumed to cause additional inflections are listed. pK_{ai} and c_i values are given in parentheses. [e] pK_a values were estimated by assuming that changes in chemical shift can be detected at pH values within ±0.5−1 unit of the pK_a of an ionizable group. [f] Value could not be obtained due to very little change in the chemical shift or weak peak intensities.

titration shift (0.5−1.5 ppm), while the C^γ chemical shifts of the acidic side chains of Asp99, Asp118, and Asp123 are almost invariable (<0.08 ppm) in the investigated pH range. As a result, the pK_a values for these aspartic acid residues could not be obtained by fitting the experimental data to a modified Henderson−Hasselbach equation.

Unfortunately, Glu178 C^δ was not observable within the whole range of pH titration. Moreover, the resonances of Glu184 C^δ, functioning as the catalytic acid or base, are increasingly difficult to assign for pH values of >6 due to the vanishing signal intensity. The explanation might be the near degeneracy of $^{13}C^\beta$ and $^{13}C^\gamma$ chemical shifts in these side chains. The concomitant strong coupling effects deteriorate the $^{13}C^\gamma$−$^{13}C^\delta$ magnetization transfer in the experiment employed here. The obtained data points for Glu184 C^δ at pH >6 imply increasing error values which lead to an uncertainty in the determination of the proper pK_a value ($5.8 < pK_a < 6.6$). As compensation, the pH-dependent chemical shifts of the closest backbone amides around Glu184 and Glu178 were considered. The amide resonances were supposed to exhibit the titration behavior of the missing reporter nuclei within a certain error range. For data analysis, the experimental data of the corresponding ^{15}N resonances of the amides were used for nonlinear regression to the modified Henderson−Hasselbach equation and the resulting pH values for the inflection points were averaged. Analogously, the pK_a value of the carboxy-terminal end of the polypeptide chain (Ser207 COOH) was determined by data analysis of the corresponding α-amino group.

Protonation Behavior and Tautomeric States of the Histidine Residues in BadX. The pH dependence of imidazole resonances was observed in the two-dimensional $H^{\delta 2}C^{\delta 2}C^\gamma$−$H^{\epsilon 1}C^{\epsilon 1}$ correlation experiment (CT-HCDCG^{His}, Figure 4) to assess the pK_a values and the tautomeric states of the four histidine residues. For all pH titration steps, the imidazole ^{13}C resonances (C^γ, $C^{\delta 2}$, and $C^{\epsilon 1}$) were assigned, and the pH dependence of the chemical shifts is presented in panels D and E of Figure 3. The increased level of line broadening of the $C^{\gamma,\delta 2}$ resonances of His32 at pH >5.5 worsened the precision of the assignment of the chemical shift values. During the course of the pH titration, all resonances of the imidazole side chain of His162 remained constant, indicating that its ionization state did not change. The question of whether the pK_a value of this buried residue is less than 3 or greater than 9 will be discussed below. Furthermore, the imidazole resonances of His32 $C^{\delta 2}$ and of His C60$^{\epsilon 1}$ showed little change in chemical shift, unlike the other resonances of their imidazole ring. As a result, the corresponding experimental data were not used for a reliable determination of pK_a values. The data analysis of His11 demonstrates one exception. The minor linear coefficient had to be assigned to the imidazole group itself, while the major one was attributed to the protonation or deprotonation process of the neighboring carboxylate side chain of Asp12.

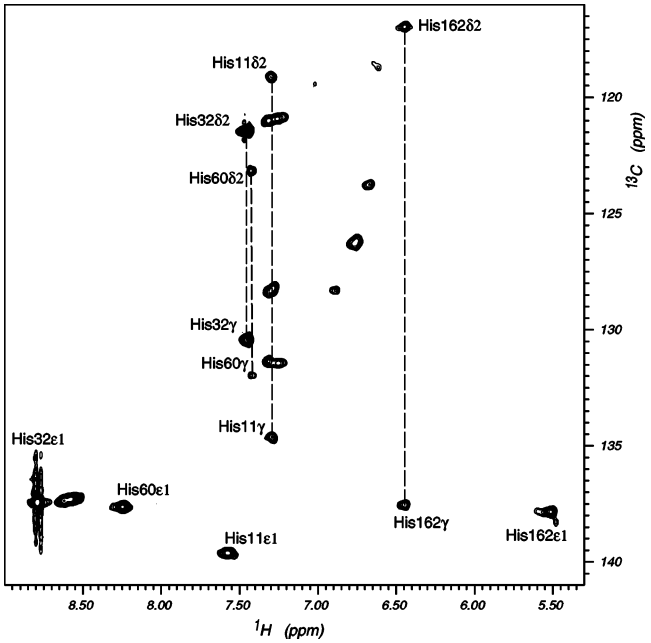

FIGURE 4: Typical CT-HCDCG^{His} spectrum of [^{15}N,^{13}C]BadX demonstrating the $H^{\delta2}C^{\delta2}C^{\gamma}-H^{\epsilon1}C^{\epsilon1}$ correlations of the four histidines. Measurements were performed for 0.5 mM [^{15}N,^{13}C]BadX in 10 mM d_3-NaOAc (pH 3.2; 5% D_2O/5% d_5-glycerol mixture) containing 50 mM $MgCl_2$.

Inspection of the $^{13}C^{\gamma}$ chemical shift−pH profile yields information about the tautomeric state of the deprotonated histidine ring because, with increasing pH, the resonance shifts upfield or downfield in proportion as the $N^{\delta1}-H$ or $N^{\epsilon2}-H$ tautomer is formed (*35*, *36*). Being deprotonated, His11, His32, and His60 prefer the $N^{\epsilon2}-H$ tautomeric state marked by the downfield shifts of the corresponding C^{γ} imidazole resonances (Figure 3D). The increased level of line broadening of His32 $C^{\gamma,\delta2}$ resonances at pH >5.5 indicates an interconversion of the two tautomeric states at intermediate rates on the NMR time scale. The obtained data points for pH 5.5−7.2 could not be subjected to nonlinear regression. Additionally, chemical shift values δ(His162 $N^{\epsilon2}$) (169.5 ppm) and δ(His162 $H^{\epsilon2}$) (12.4 ppm) led to the conclusion that His162 is deprotonated and the $N^{\epsilon2}-H$ tautomeric state prevails (*29*). This confirms the previously reported finding obtained with an alternative NMR method (*37*). All three $^{13}C^{\delta2}$ chemical shifts are <122 ppm, and a predominance of the $N^{\epsilon2}-H$ tautomers is indicated.

DISCUSSION

Standard pK_a values of titratable amino acid side chains can be measured for short oligopeptides serving as model compounds (*33*, *34*). Deviations from these reference values can be observed during the titration of proteins. This results either from structural interactions (hydrogen bonds and salt bridges) or from interactions with neighboring side chains in an environment with a low dielectric constant such as the core regions of globular proteins. Among family 11 xylanases, the aromatic interactions and the hydrophobic contacts form clusters that are highly similar (*38*, *39*), which are concentrated not only in the core of the enzymes but also in the sandwich fold structure of the catalytic domain. Besides the sterical hindrance caused by the additional hydroxymethyl group of the glycosyl moieties of the cellulose, the rather hydrophobic environment favors the bonding of xylan over the more hydrophilic cellulose fibers. The packing of the catalytic side chains between the aromatic and hydrophobic residues results in a perpendicular orientation of the carboxylate groups toward the substrate. In Figure 2, the titratable groups of BadX for pH 3−9 according to their location in the crystal structure are depicted. Only four of the 15 carboxylate side chains (Asp5, Asp90, Glu56, and Glu126; see also Table 1) exhibit ideal titration behavior according to the classical Henderson−Hasselbach equation. These four carboxylate groups are positioned on loops and are solvent-exposed and distant from all other titratable groups in BadX. Their apparent pK_a values correspond exactly to intrinsic values obtained for model compounds (*33*, *34*). However, the pH titration profiles of the other carboxylate groups deviate considerably from profiles expected for residues, which are not significantly influenced by the protein environment. Mutual interactions appear to be reasonable because the carboxylate groups are not scattered uniformly over the protein surface, but most of them are grouped together in the substrate binding cleft (see Figure 2A) among the aromatic residues (see also Figure 8A).

BadX contains one histidine (His162) and one aspartate (Asp99), which are completely buried within the hydrophobic core of the enzyme. This structural motif together with the stabilizing interactions between the conserved residues has recently been characterized with the homologous *Bacillus circulans* xylanase (BCX) (*40*, *41*). Two aspartic acid residues (Asp118 and Asp123) are located in the vicinity of this core but have limited solvent accessibility (Table 1). All four titratable residues of recombinant BadX are deprotonated in the investigated pH range of 3.2−8.7. With the assumption that changes in chemical shift can be detected at pH values within ±0.5 unit of the pK_a of an ionizable group, the pK_a values of the buried residues are <2.7. Invariant chemical shift values δ(His162 $N^{\epsilon2}$) (169.5 ppm) and δ(His162 $H^{\epsilon2}$) (12.4 ppm) which can be detected in all pH-dependent $^{15}N-^{1}H$ TROSY-HSQC spectra suggest that His162 exists in the neutral $N^{\epsilon2}$ tautomeric form, and the exchange rate of the $H^{\epsilon2}$ with the solvent molecules is retarded. This observation is supported by the inspection of the crystal structure. His162 $N^{\delta1}$ is involved in a hydrogen bond with the hydroxyl group of Ser146, and a second hydrogen bond is formed between the $N^{\epsilon2}-H$ group and a water molecule. The abnormally low pK_a of His162 undoubtedly reflects the buried hydrophobic environment of the imidazole ring within the enzyme. His162 contacts several nonpolar residues, including Val98, Ile115, Tyr122, and Ile157, which are highly conserved. The negative charge of Asp99 is stabilized by a hydrogen bond to the phenolic O^{η} of Tyr122 and by the salt bridge to the positively charged guanidinium group of Arg122. The low pK_a value of Asp123 can be rationalized by the interactions with the positive charges of Arg105 and Arg149. Generally, the resonances of the backbone amides in the neighborhood of the four nontitratable side chains remain unaffected during the course of the pH titration, allowing the conclusion that the conformation of this region is invariant (Figure 2B).

Despite His162, the side chains of His11 and His32 are exposed to the solvent. Together with Asp12, they are grouped together at the entrance of the substrate binding cleft, but their orientations are directed toward the convex outside.

The relative positions of His11, His32, and Asp12 can be described as a triangle with two sides equal in length. Asp12 is at the top 5.5 Å from either histidine, and the distance between His11 and His32 is approximately 8.2 Å. The data analysis of the corresponding pH-dependent resonances displays normal pK_a values, but titration curves exhibit additional inflection points due to the mutual electrostatic interactions. The titration curve of His32 $C^{\delta 2}$ has a very small dispersion of chemical shifts ($\delta_a - \delta_b$) and is dominated by the interaction of Asp12. Therefore, the fitted pK_a value is solely attributed to the carboxylate group and not to the reporter nucleus itself. There is no evidence that Asp12 has a favorable interaction with only one of the histidine side chains. Therefore, the additional titration event is assigned to mutual interactions with both histidines within the estimated error values.

The His60−Glu167 group is located on the side opposite the active site cleft. Both side chains fill a small hollow on the surface of the protein. The convex outside is formed by β-sheet A, and the sides of the hollow are marked by α-helices 1 and 2. The proximity of both side chains (His60 $N^{\epsilon 2}$−Glu167 O^{ϵ} distance of 2.8 Å), the sharing of a hydrogen bond, leads to a strong interdependence of both titratable groups. The titration curves of both side chains lack evident inflection points, which separate protonation or deprotonation steps from each other. For His60, the negative charge of the side chain carboxylate Glu167 would be expected to stabilize the protonated, positively charged imidazole ring; therefore, the apparent histidine pK_a would be elevated beyond 7.0 in comparison to that of an unaffected model compound. However, the titration curves of His60 in panels D and E of Figure 3 do not present evidence that the pK_a value is between 7 and 8.7. This leads to the question of whether the apparent pK_a value is higher than 8.7 or the inflection points around pH 4 mark the corresponding pK_a value. A possible low pK_a value for His60, despite the electrostatic influence of Glu167, provides a hint of an unusual microenvironment. The X-ray structure and the sequence alignment show that His60 is mostly surrounded by conserved, hydrophobic residues. His60 acts as a "lid" on a hydrophobic site with a low dielectric constant and has limited solvent accessibility (Table 1). It is an energetically unfavorable process of transferring a charged proton from the highly polar aqueous solvent to the hydrophobic microenvironment in which the dielectric constant is estimated to be much lower (*42*). Further inspection reveals that the imidazole ring is located at the N-terminus of small α-helix 1. It is well-documented that α-helices have a macroscopic dipolar character arising from the parallel alignment of the dipolar peptide bonds of the helix. Therefore, His60 could be under the influence of a slight positive charge (*43*−*45*). Though a strong interdependence to Glu167 is evident, the conclusion is that the pK_a value of His60 is estimated to be within a range of 4.0−4.3, adding an extended error value. The real pK_a value is probably at the upper limit, possibly around 4.3.

The ligand binding site of BadX comprises a cluster of charged residues on the interior β-sheet, including Asp15, Glu17, Asp21, Glu178, and the catalytic dyad, Glu94 and Glu184. A closer inspection reveals that the acidic residues can be divided into two groups corresponding to the subsites for the sugar moieties: Asp15, Glu17, and Glu178 in subsite −2 and the catalytic dyad in subsite −1. Asp21 cannot be attributed to one of the groups because none of the other acidic residues is located within 7 Å, but the examination of the titration curve of Asp21 C^{γ} reveals an unusual titration behavior. The resonances undergo a substantial small pH titration shift and reach a maximum value at pH 5. For higher pH values, the C^{γ} resonances experience a pronounced reverse shift. The verification of the data analysis allows the correlation with additional titration events between 5.3 and 6.9, contributing to the extraordinary chemical shift−pH profile of Asp21 C^{γ}. Because of its singular position, the observation cannot be explained with respect to direct interaction with a nearby titratable group, which should have a pK_a value in the corresponding range (p$K_a \approx 5.0-7.2$). To investigate the long-range nature of the interaction, the pH-dependent resonances of surrounding amide groups were analyzed.

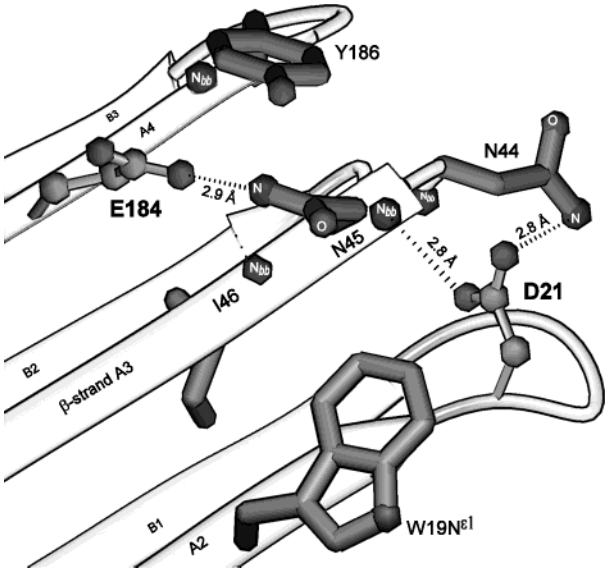

FIGURE 5: Ribbon representation showing the position of Asp21 and the Brønsted acid or base Glu184, as well as selected neighboring side chains. Dashed lines illustrate the distances for possible hydrogen bonds. Backbone amides, whose chemical shift titration curves (Figure 5) were used as probes to investigate electrostatic interactions, are drawn as spheres.

Figure 5 illustrates that the carboxylate side chain of Asp21 is involved in two hydrogen bonds: one bond to the side chain amide of Asn44 $N^{\delta 2}$ and one to the backbone amide of Asn45. A comparison of corresponding titration curves of Asn45 and the side chain of Asp21 exhibits striking similarities (Figure 6). The inflection points can be observed in each of the three curves, indicating a strong interdependence of titration behavior. Figure 6 shows that several backbone amide resonances in the vicinity of Asn45 experience significant chemical shift changes, which can be attributed to the ionization of either Asp21 or Glu184, but in comparison to the other amide groups, the $^1H^N$ resonances of Asn45 display the strongest dependence upon deprotonation of the resonances of the acidic side chains (see also Figure 1).

In general, the side chain of Asn45 has an important function during the catalytic reaction. Asn45 shares a hydrogen bond with the carboxylate group of Glu184, which acts as the Brønsted acid or base during the catalytic reactions. After the formation of the glycosyl−enzyme

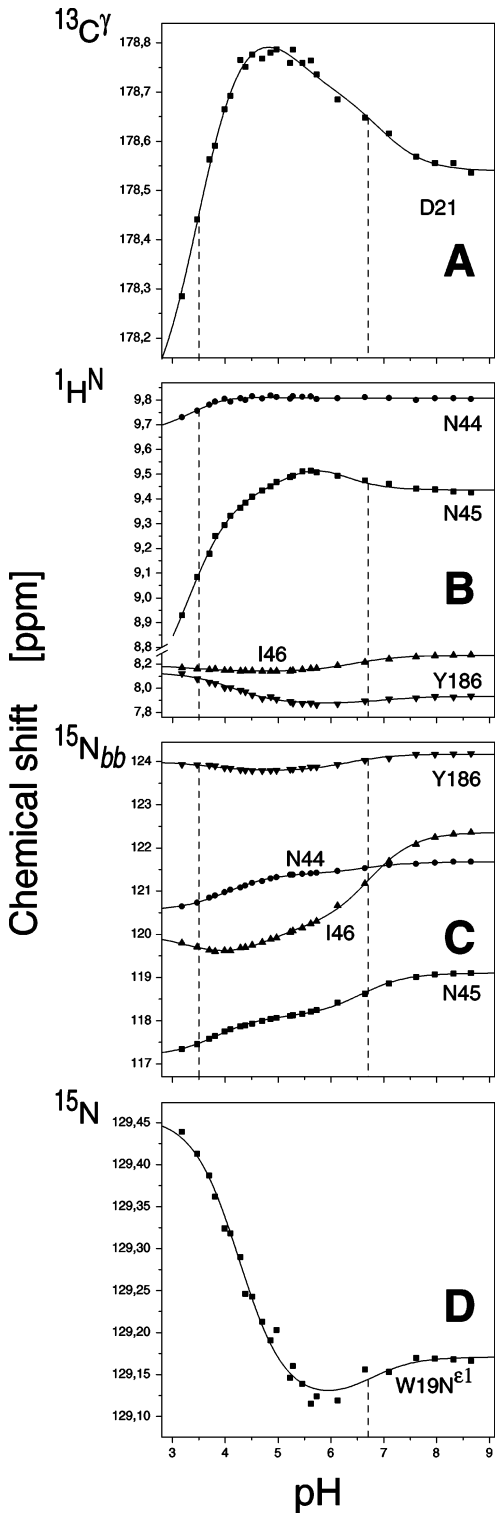

FIGURE 6: Chemical shift titration curves of selected neighboring groups of Asp21 (Figure 5) in the pH range of 3.2−8.7. Data points were taken from two-dimensional $^{1}H-^{13}C$ and $^{1}H-^{15}N$ correlation NMR spectra. Symbols represent experimental data points. (A) Representation of nonlinear least-squares fits to the modified Henderson−Hasselbach equation according to the noninteracting model with three [$j = 3$; D21 C^{γ} (■)] apparent pK_a values. (B and C) Representation of the least-squares best fit to the same equation with one [$j = 1$; N44 H^N (●)], two [$j = 2$; Trp19 $N^{\epsilon 1}$ (■), N44 N_{bb} (●), N45 N_{bb} (●), I46 H^N (▲), and Y186 H^N/N_{bb} (▼)], or three [$j = 3$; Asn45 H^N (■) and I46 N_{bb} (▲)] inflection points correlating to the protonation and deprotonation process of nearby residues Asp21 and Glu184. Dashed lines illustrate the inflection points showing the interdependence on the titration events of the acidic side chains of Asp21 and Glu184.

intermediate, Asn45 supports the nucleophilic attack by establishing a hydrogen bond with the reactive water molecule (*11*, *46*, *47*).

For a possible electrostatic interaction, Glu184 would have a proper pK_a value of 6.5 but its carboxyl group is at a distance of 9 Å. As a consequence, the unusual titration profile of Asp21 C^{γ} is interpreted with the influence of Glu184 via two hydrogen bonds with Asn45 as the mediator. With Asn45 playing this role, the chemical shift−pH profile of its backbone amide reflects the interactions of both carboxylate side chains. On one hand, the inflection points at pH 6.8 (H^N) and pH 6.6 (N_{bb}), respectively, represent the dependence on Glu184 and on the other hand with pH 3.3 (H^N) and pH 3.7 (N_{bb}), respectively, the interaction with Asp21 (3.5).

This result gives additional information about the pivotal role of amino acid 45, which is related to the catalytic pH optimum of the family 11 xylanases. In a recent study (*39*), an alignment of 82 amino acid sequences revealed that the presence of asparagines correlates with so-called "alkaline" xylanases such as BadX or BCX, or aspartates in those with a more acidic pH optimum, e.g., xylanase I from *Aspergillus niger* (*47*). A substitution of Asn45 with an aspartic acid residue would lead to the formation of a rather short and strong hydrogen bond with Glu184. It has been proposed for the N35D mutant of BCX that homologous residue Asp35 and Brønsted acid or base catalyst Glu172 exhibit a "reverse protonation" mechanism due to the subsequent sharing of a single proton. The catalytic action takes place if Asp35, with the lower pK_a value, is protonated, while the nucleophile Glu78, with the higher pK_a value, is deprotonated (*48*).

It is evident that the titration profiles of Asp21 C^{γ} or Asn45 H^N cannot be attributed to mere electrostatic interactions, which would result in a simple monotonic slope. Adding negative charges to the protein by gradual removal of protons leads to an increase in electronegativity. Therefore, the neighboring amide would be more and more deshielded with an increased net charge (*19*). However, the alternation between positive and negative slopes of pH titration profiles indicates a more complex mechanism. Rather, such reverse shifts are supposed to be the consequence of a simultaneous reorganization of side chain conformational space at pH ≈6 and/or an overall change in the hydrogen network in the substrate binding cleft. Changes in the backbone conformation can be excluded since relaxation measurements with the homologous xylanase from *B. circulans* suggest that family 11 xylanases are compact globular proteins with very limited backbone flexibility (*49*). Similar results were published for another family 11 xylanase (XYNII) from *Trichoderma reesei* (*50*) which was crystallized at pH 5.0 and 6.5 (Protein Data Bank entries 1XYO and 1XYP, respectively). The rms difference between the two crystal structures was calculated from the positions of all C^{α} atoms, and the reported value of 0.148 Å indicates that the backbone conformation remains extensively constant. The only exception is a change of ∼0.6 Å in the position of the "cord" (residues 96−102) which partly closes the active site cleft at one side.

The hypothesis of a "reshuffling" of side chain conformational space at pH ≈6 and the hydrogen bond pattern is supported by the pronounced chemical shift changes of backbone amides located in the cleft (Figures 2A and 7). It can also be rationalized with the titration profile of the indole

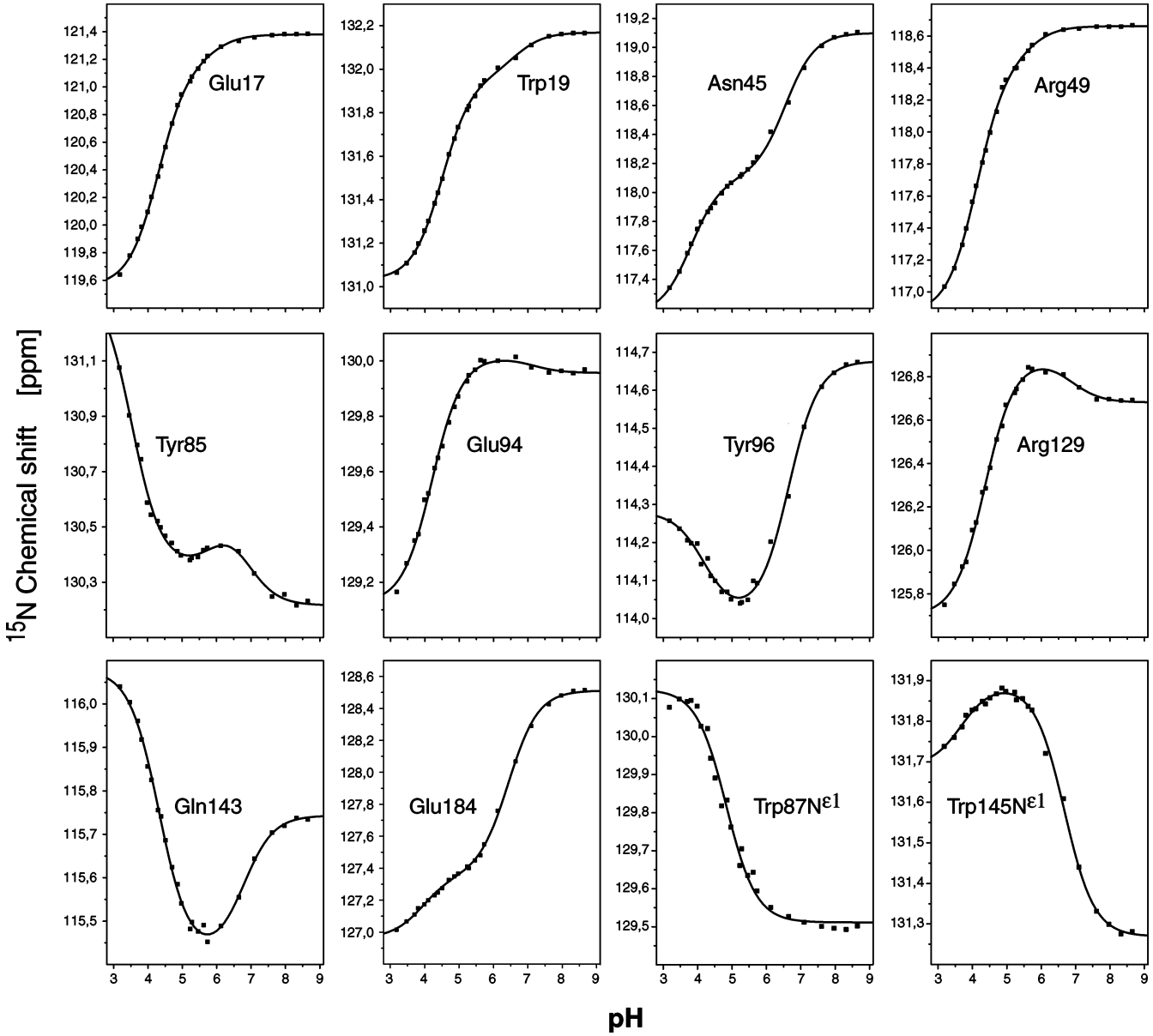

FIGURE 7: pH-dependent chemical shift values of backbone amides involved in substrate binding. Experimental data points (■) were taken from two-dimensional $^{15}N-^{1}H$ TROSY-HSQC spectra. The solid lines are the least-squares best fits to the modified Henderson−Hasselbach equation with one ($j = 1$; W87 $N^{\epsilon 1}$), two ($j = 2$; E17, W19, N45, R49, E94, Y96, R129, Q143, E184, and W145 $N^{\epsilon 1}$), or three inflection points ($j = 3$; Y85).

side chain atom Trp19 $N^{\epsilon 1}$ (Figure 6D), which is 9.9 Å from the carboxyl of Glu184. It reaches a minimum number of chemical shifts, and then it is correlated to Glu184 with a minor reverse shift at pH 6.7. Generally, the electronic shielding depends mainly on the short-range contribution in the vicinity of the inspected nucleus. Changes in the heteroaromatic system of the indole are negligible, and therefore, long-range contributions are to be considered. Törrönen et al. (*50*) showed for XYNII that the side chain conformations of homologous residues Asn44 and Trp18 did not change between pH 5.0 and 6.5. However, Glu177, which is the corresponding Brønsted acid of the catalytic dyad of XNYII, revealed a large displacement of 2.8 Å related to the position of the C^{δ} atom. The hydrogen bond between the side chain of Glu177 and the side chain amide of Asn44 $N^{\delta 2}$ is stretched from 3.4 to 3.7 Å during this pH-induced conformational change. A similar movement of the side chain of Glu184 in BadX and the consecutive rearrangement of nearby side chains could alter the surrounding electrical field or the magnetic anisotropies of the discussed residues, which leads to the observed reverse shift of Trp19, Asp21, and Asn45 at higher pH values.

The side chain pH titration profile of Asp15, which is located at the opposite side of the substrate binding cleft, shows a similar dependence around pH 6−7. At lower pH values, the titration curve of Asp15 C^{γ} displays a pK_a of 3.4, which is modestly lower than values for model compounds. This can be rationalized as a perturbation caused by the other acidic side chains of subsite −2, Glu17 (pK_a = 4.3) and Glu178 (pK_a = 4.1), which are likely to cause the second apparent pK_a value of 4.5. A third titration event (pH 6.7) is interpreted as a consequence of the mentioned change in side chain conformations and hydrogen network.

Subsite −1 of BadX contains the catalytic dyad, Glu94 and Glu184, which is an analogous example of coupled titration behavior that has already been characterized for BCX

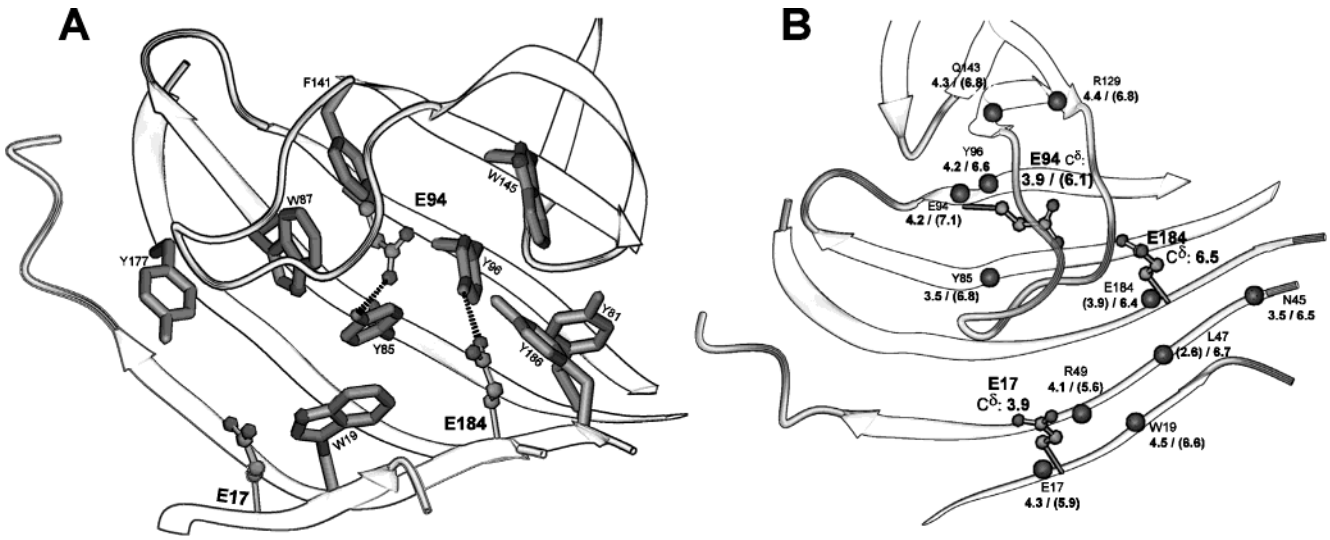

FIGURE 8: Structural environment of the active site represented as a ribbon diagram. (A) Aromatic−hydrophobic microenvironment of the acidic residues located in the substrate binding cleft. Dashed lines illustrate possible hydrogen bonds. (B) Titration behavior of backbone amides of active site residues which are involved in xylan fiber binding as observed recently (*11*). Spheres represent the backbone amide nitrogen atoms whose corresponding titration data were analyzed to show the interdependence on the protonation state of the nearby acidic side chains. Numbers annotate inflection points or apparent pK_a values. In parentheses are values with the smaller linear coefficient (c_i) of the regression analysis.

(*51*). Here, the pH-dependent resonances of Glu94 C^{δ} show a pronounced biphasic profile, allowing a fit of two apparent pK_a values. The first pK_a value (3.9) is attributed to Glu94 itself, while the second (6.1) reflects the protonation or deprotonation process of the opposite Glu184 (Glu94 $O^{\epsilon 2}$−Glu184 $O^{\epsilon 1}$ distance of 5.7 Å). This result is in good agreement with the reported pH dependence of k_{cat}/K_m for the hydrolysis of a substrate analogue by BadX which follows a bell-shaped curve with an optimum value at pH 5.6 (*17*). Glu94 with its pK_a value of 3.9 is able to perform the nucleophilic attack because it is deprotonated for more than 99% at pH > 6. The very shallow titration curve of Glu184 could only be used for data analysis with pH values of <5.5. The correlated pK_a of 4.4 is to be attributed to the influence of Glu94. The pK_a of Glu184 itself was determined indirectly via neighboring backbone amides. These resonances exhibited quite similar profiles, yielding an average pK_a value of 6.5 for Glu184. This result also corresponds with the reported enzymatic activity of BadX (*17*). Glu184 is protonated to a sufficient extent at modestly elevated pH values and therefore is able to initiate cleavage by donating its proton to the bridging oxygen atom of the β-1,4 glycosidic bond.

The reciprocal relationship of the pK_a values can be analyzed by considering mutual electrostatic repulsion of like charges. An interaction of two neighboring carboxylate groups increases one pK_a value, thus preventing the unfavorable Coulombic energetics. Unfortunately, no simple reasoning can be provided to explain why the pK_a value of Glu184 is increased and not that of Glu94. It might be more likely that Glu94 is better stabilized due to the closer location of the positive charge of Arg129 (distance of 5.3 Å), and therefore, the pK_a of Glu184 increases (distance to Arg129 of 6.7 Å) (*51*, *52*). An explanation for the strong perturbation of *both* carboxylate groups is the unusual hydrophobic microenvironment created by several aromatic residues located in the active site cleft (Figure 8A).

At least the asymmetric titration behavior can be correlated with the chemical shift−pH profiles of aromatic indole nitrogens Trp87 $N^{\epsilon 1}$ (inflection point at pH 4.8) and Trp145 $N^{\epsilon 1}$ (inflection point at pH 6.7; see Figure 7). The carboxylate group of Glu94 is equidistant from both tryptophan side chains (5.9 and 6.2 Å), which is comparable with the distance geometry of Glu184 (5.7 Å to Trp87 and 6.5 Å to Trp145). The protonation or deprotonation process of Glu94 dominates the chemical shift−pH profile of Trp87 $N^{\epsilon 1}$, while Glu184 rules over that of Trp145 $N^{\epsilon 1}$. Direct electrostatic interaction seems to be less crucial because of the pairlike distance geometry. It is more probable that the asymmetric interaction is mediated via hydrogen bonds and $\pi-\pi$ stacking. Glu94 O^{ϵ} forms a bridge to the phenolic oxygen atom of Tyr85 (O^{η}) with a hydrogen bond and Glu184 O^{ϵ} to Tyr96 O^{η} (see Figure 8A). The plane of Trp87 is perpendicular to that of Tyr85, but Tyr96 is parallel to Trp145 due to $\pi-\pi$ stacking. The conclusion is if an ionization step of one carboxylate group leads to a new equilibrium of side chain conformations or modifies the hydrogen bond to the corresponding tyrosine, this effect could be transferred to the neighboring indole. The shifted aromatic ring planes would alter their influence via the magnetic anisotropy on the indole $N^{\epsilon 1}$ resonances. This argument could explain that the ionization of Glu94 dominates the chemical shift−pH profile of Trp87 via Tyr85, while Glu184 has a strong influence over Trp145 via Tyr96. An analogous situation was described for the active site of XYNII with the homologous groups of residues Glu86 (BadX residue, Glu94), Tyr77 (Tyr85), and Trp79 (Trp87) and Glu177 (Glu184), Tyr88 (Tyr96), and Trp138 (Trp145). The two crystal structures of XNYII reveal minor changes in the side chain conformations of Glu86, Tyr77, and Trp79 but major changes for Glu177, Tyr88, and Trp138. These findings support the hypothesis that the correlation of chemical shift−pH profiles among the two homologous groups of BadX could be based on the reshuffling of side chain orientations and the hydrogen network.

To complete the investigation of the active site, all ^{15}N amide titration curves of the backbone residues which take part in substrate binding were inspected (Figure 7). Most of the titration curves exhibit biphasic behavior with two distinct inflection points, which correspond to the nearby acidic side chains of Glu17, Glu94, and Glu184.

Data analysis with nonlinear regression resulted in two separate groups of inflection points. The first group reflects the titration behavior of Glu17 and Glu94 with values around pH 4.0 ± 0.3. The second group can be attributed to Glu184 with values around pH 6.5 ± 0.2. To illustrate the interdependence between backbone amides and carboxylate groups, the corresponding nitrogen atoms are drawn in Figure 8B as van der Waals spheres and inflection points, respectively. pK_a values are annotated.

Simple ascending slopes of the titration profiles, which can be observed for backbone amides of Glu17, Trp19, Asn45, Arg49, and Glu184, could be explained in terms of electrostatic interaction. The alternation between positive and negative slopes of pH titration profiles of Tyr85, Glu94, Tyr96, Arg129, and Gln143 could be rationalized as the perturbation, caused by the reorientation of side chains and the reorganization of the hydrogen network at pH ≈6, dominates mere electrostatic interactions for these residues. The slope of the chemical shift−pH profile of the backbone amide Tyr85 is even more peculiar since it reveals two changes in the mathematical signs. Maybe this is the result of its inherent flexibility. The side chain of Tyr85 is located at the border between subsites −1 and −2. Once the substrate had bound, the phenolic oxygen atom was proposed to able to interact with *both* sugar moieties (*11*).

In summary, ^{1}H and ^{13}C NMR spectroscopy revealed the Coulombic interactions of carboxylate and histidines groups of BadX. Combining these results with a thorough data analysis of backbone amide and tryptophan side chain resonances, which can routinely be obtained by $^{15}N-^{1}H$ TROSY-HSQC spectra, gave additional information about mutual long-range interactions.

This study confirms that the protonation and deprotonation process of Glu184 in BadX marks a midpoint of a concerted reaction, which takes place in the entire substrate binding cleft. It is very likely that the side chains located in the active site adopt a new conformation and/or the extensive hydrogen network arranges itself to a new equilibrium. The chemical shift−pH profiles of tryptophan indole nitrogen resonances suggest that side chain conformation and aromatic−aromatic interactions should be considered. Maybe the hydrogen bonds of the side chains of Glu184 and Glu94 to their neighboring tyrosine hydroxyl groups serve as a starting point for long-range interactions. A new local conformation could be conveyed via $\pi-\pi$ stacking effects to the aromatic hydrophobic microenvironment of the whole active site. This might explain why Glu184 influences the chemical shifts of the reporter nuclei with a distance up to 10 Å. As shown for Asn45 which is pivotal for the more alkaline catalytic optimum of BadX, hydrogen bonds can mediate decisive interactions.

The implication of these results on the theoretical analysis of the electrostatic properties of BadX or proteins in general suggests that simplifying assumptions during structure-based predictions should be reconsidered. Further investigations, which compare electrostatic interactions derived from theoretical calculations with the experimental data presented here, will be discussed in a follow-up publication. The neglect of conformational changes or the position of hydrogen bonds, which can change during the course of pH variation, may lead to the deviation of calculated pK_a values.

ACKNOWLEDGMENT

The recombinant enzyme BadX was produced in collaboration with Novo-Nordisk A/S (Bagsvaerd, Denmark). We extend our thanks to the reviewers for the valuable advice regarding the pH-dependent crystal structures.

REFERENCES

1. Harris, T. K., and Turner, G. J. (2002) Structural basis of perturbed pK_a values of catalytic groups in enzyme active sites, *IUBMB Life 53*, 85−98.
2. Forsyth, W. R., Antosiewicz, J. M., and Robertson, A. D. (2002) Empirical relationships between protein structure and carboxyl pK_a values in proteins, *Proteins 48*, 388−403.
3. Spitzner, N., Löhr, F., Pfeiffer, S., Koumanov, A., and Rüterjans, H. (2001) Ionization properties of titratable groups in ribonuclease T1. I. pK_a values in the native state determined by two-dimensional heteronuclear NMR spectroscopy, *Eur. Biophys. J. 30*, 186−197.
4. Koumanov, A., Spitzner, N., Rüterjans, H., and Karshikoff, A. D. (2001) Ionization properties of titrable groups in ribonuclease T1. II. Electrostatic analysis, *Eur. Biophys. J. 30*, 198−206.
5. Giletto, A., and Pace, C. N. (1999) Buried, charged, non-ion-paired aspartic acid 76 contributes favorably to the conformational stability of ribonuclease T1, *Biochemistry 38*, 13379−13384.
6. Warshel, A., and Papazyan, A. (1998) Electrostatic effects in macromolecules: fundamental concepts and practical modeling, *Curr. Opin. Struct. Biol. 8*, 211−217.
7. Ullmann, G. M., and Knapp, E. W. (1999) Electrostatic models for computing protonation and redox equilibria in proteins, *Eur. Biophys. J. 28*, 533−551.
8. Simonson, T. (2001) Macromolecular electrostatics: continuum models and their growing pains, *Curr. Opin. Struct. Biol. 11*, 243−252.
9. Schutz, C. N., and Warshel, A. (2001) What are the dielectric "constants" of proteins and how to validate electrostatic models? *Proteins 44*, 400−417.
10. Fitch, C. A., Karp, D. A., Lee, K. K., Stites, W. E., Lattman, E. E., and Garcia-Moreno, E. B. (2002) Experimental pK_a values of buried residues: analysis with continuum methods and role of water penetration, *Biophys. J. 82*, 3289−3304.
11. Sabini, E., Sulzenbacher, G., Dauter, M., Dauter, Z., Jorgensen, P. L., Schulein, M., Dupont, C., Davies, G. J., and Wilson, K. S. (1999) Catalysis and specificity in enzymatic glycoside hydrolysis: a 2.5 Å conformation for the glycosyl-enzyme intermediate revealed by the structure of the *Bacillus agaradhaerens* family 11 xylanase, *Chem. Biol. 6*, 483−492.
12. Wakarchuk, W. W., Campbell, R. L., Sung, W. L., Davoodi, J., and Yaguchi, M. (1994) Mutational and crystallographic analyses of the active site residues of the *Bacillus circulans* xylanase, *Protein Sci. 3*, 467−475.
13. Gruber, K., Klintschar, G., Hayn, M., Schlacher, A., Steiner, W., and Kratky, C. (1998) Thermophilic xylanase from *Thermomyces lanuginosus*: high-resolution X-ray structure and modeling studies, *Biochemistry 37*, 13475−13485.
14. Wouters, J., Georis, J., Engher, D., Vandenhaute, J., Dusart, J., Frere, J. M., Depiereux, E., and Charlier, P. (2001) Crystallographic analysis of family 11 endo-β-1,4-xylanase Xyl1 from *Streptomyces* sp. S38, *Acta Crystallogr. D57*, 1813−1819.
15. Davies, G. J., Wilson, K. S., and Henrissat, B. (1997) Nomenclature for sugar-binding subsites in glycosyl hydrolases, *Biochem. J. 321*, 557−559.
16. Törrönen, A., and Rouvinen, J. (1997) Structural and functional properties of low molecular weight endo-1,4-β-xylanases, *J. Biotechnol. 57*, 137−149.
17. Poon, D. K., Webster, P., Withers, S. G., and McIntosh, L. P. (2003) Characterizing the pH-dependent stability and catalytic mechanism of the family 11 xylanase from the alkalophilic *Bacillus agaradhaerens*, *Carbohydr. Res. 338*, 415−421.
18. Product Sheet, N. A. S. P. (2002) Pulpenzyme HC.

19. de Dios, A. C., Pearson, J. G., and Oldfield, E. (1993) Secondary and Tertiary Structural Effects on Protein NMR Chemical Shifts: An ab Initio Approach, *Science 260*, 1491−1496.
20. Szilagyi, L. (1995) Chemical shifts in proteins come of age, *Prog. Nucl. Magn. Reson. Spectrosc. 27*, 325−443.
21. Betz, M., Löhr, F., Wienk, H., and Rüterjans, H. (2002) Letter to the Editor: ^{1}H, ^{13}C and ^{15}N chemical shift assignment of *Bacillus agaradhaerens* family 11 xylanase, *J. Biomol. NMR 23*, 333−334.
22. Gill, S. C., and von Hippel, P. H. (1989) Calculation of protein extinction coefficients from amino acid sequence data, *Anal. Biochem. 182*, 319−326.
23. Pervushin, K., Riek, R., Wider, G., and Wuthrich, K. (1997) Attenuated T2 relaxation by mutual cancellation of dipole−dipole coupling and chemical shift anisotropy indicates an avenue to NMR structures of very large biological macromolecules in solution, *Proc. Natl. Acad. Sci. U.S.A. 94*, 12366−12371.
24. Powers, R., Gronenborn, A. M., Clore, G. M., and Bax, A. (1991) Three-Dimensional Triple-Resonance NMR of ^{13}C/^{15}N-Enriched Proteins using Constant-Time Evolution, *J. Magn. Reson. 94*, 209−213.
25. Grzesiek, S., and Bax, A. (1993) The Origin and Removal of Artifacts in 3D HCACO Spectra of Proteins Uniformly Enriched with ^{13}C, *J. Magn. Reson., Ser. B 102*, 103−106.
26. Yamazaki, T., Nicholson, L. K., Torchia, D. A., Wingfield, P., Stahl, S. J., Kaufmann, J. D., Eyermann, C. J., Hodge, C. N., Lam, P. Y., Ru, Y., Jadhav, P. K., Chang, C. H., and Weber, P. C. (1994) NMR and X-ray evidence that the HIV protease catalytic aspartyl groups are protonated in the complex formed by the protease and a non-peptide cyclic urea-based inhibitor, *J. Am. Chem. Soc. 116*, 10791−10792.
27. Wishart, D. S., Bigam, C. G., Yao, J., Abildgaard, F., Dyson, H. J., Oldfield, E., Markley, J. L., and Sykes, B. D. (1995) ^{1}H, ^{13}C and ^{15}N chemical shift referencing in biomolecular NMR, *J. Biomol. NMR 6*, 135−140.
28. Shrager, R. I., Cohen, J. S., Heller, S. R., Sachs, D. H., and Schechter, A. N. (1972) Mathematical models for interacting groups in nuclear magnetic resonance titration curves, *Biochemistry 11*, 541−547.
29. Blomberg, F., Maurer, W., and Rüterjans, H. (1977) Nuclear magnetic resonance investigation of ^{15}N-labeled histidine in aqueous solution, *J. Am. Chem. Soc. 99*, 1849−1859.
30. Motulsky, H. J., and Ransnas, L. A. (1987) Fitting curves to data using nonlinear regression: a practical and nonmathematical review, *FASEB J. 1*, 365−374.
31. Ayed, A., Mulder, F. A., Yi, G. S., Lu, Y., and Kay, L. E. (2001) Latent and active p53 are identical in conformation, *Nat. Struct. Biol. 8*, 756−760.
32. Seavey, B. R., Farr, E. A., Westler, W. M., and Markley, J. L. (1991) A rational database for sequence-specific protein NMR data, *J. Biomol. NMR 1*, 217−236.
33. Keim, P., Vigna, R. A., Morrow, J. S., Marshall, R. C., and Gurd, F. R. (1973) Carbon 13 nuclear magnetic resonance of pentapeptides of glycine containing central residues of serine, threonine, aspartic and glutamic acids, asparagine, and glutamine, *J. Biol. Chem. 248*, 7811−7818.
34. Richarz, R., and Wüthrich, K. (1978) Carbon-13 NMR chemical shifts of the common amino acid residues measured in aequous solutions of the linear tetrapeptides H-Gly-Gly-X-L-Ala-OH, *Biopolymers 17*, 2133−2141.
35. Reynolds, W. F., Peat, I. R., Freedman, M. H., and Lyerla, J. R., Jr. (1973) Determination of the tautomeric form of the imidazole ring of L-histidine in basic solution by carbon-13 magnetic resonance spectroscopy, *J. Am. Chem. Soc. 95*, 328−331.
36. Walters, D. E., and Allerhand, A. (1980) Tautomeric states of the histidine residues of bovine pancreatic ribonuclease A. Application of carbon 13 nuclear magnetic resonance spectroscopy, *J. Biol. Chem. 255*, 6200−6204.
37. Sudmeier, J. L., Bradshaw, E. M., Haddad, K. E., Day, R. M., Thalhauser, C. J., Bullock, P. A., and Bachovchin, W. W. (2003) Identification of histidine tautomers in proteins by 2D ^{1}H/^{13}C-(δ2) one-bond correlated NMR, *J. Am. Chem. Soc. 125*, 8430−8431.
38. Georis, J., de Lemos, E., Lamotte-Brasseur, J., Bougnet, V., Devreese, B., Giannotta, F., Granier, B., and Frere, J. M. (1999) An additional aromatic interaction improves the thermostability and thermophilicity of a mesophilic family 11 xylanase: structural basis and molecular study, *Protein Sci. 9*, 466−475.
39. Sapag, A., Wouters, J., Lambert, C., de Ioannes, P., Eyzaguirre, J., and Depiereux, E. (2002) The endoxylanases from family 11: computer analysis of protein sequences reveals important structural and phylogenetic relationships, *J. Biotechnol. 95*, 109−131.
40. Plesniak, L. A., Connelly, G. P., Wakarchuk, W. W., and McIntosh, L. P. (1996) Characterization of a buried neutral histidine residue in *Bacillus circulans* xylanase: NMR assignments, pH titration, and hydrogen exchange, *Protein Sci. 5*, 2319−2328.
41. Joshi, M. D., Hedberg, A., and McIntosh, L. P. (1997) Complete measurement of the pK_a values of the carboxyl and imidazole groups in *Bacillus circulans* xylanase, *Protein Sci. 6*, 2667−2670.
42. Rashin, V., and Honig, B. (1985) Reevaluation of the Born model of ion hydration, *J. Phys. Chem. 89*, 5588−5593.
43. Wada, A. (1976) The α-Helix as an electric macro-dipole, *Adv. Biophys. 9*, 1−63.
44. Hol, W. G., van Duijnen, P. T., and Berendsen, H. J. (1978) The α-helix dipole and the properties of proteins, *Nature 273*, 443−446.
45. Perutz, M. F., Gronenborn, A. M., Clore, G. M., Fogg, J. H., and Shih, D. T. (1985) The pK_a values of two histidine residues in human haemoglobin, the Bohr effect, and the dipole moments of α-helices, *J. Mol. Biol. 183*, 491−498.
46. Törrönen, A., and Rouvinen, J. (1995) Structural comparison of two major endo-1,4-xylanases from *Trichoderma reesei*, *Biochemistry 34*, 847−856.
47. Krengel, U., and Dijkstra, B. W. (1996) Three-dimensional structure of endo-1,4-β-xylanase I from *Aspergillus niger*: molecular basis for its low pH optimum, *J. Mol. Biol. 263*, 70−78.
48. Joshi, M. D., Sidhu, G., Pot, I., Brayer, G. D., Withers, S. G., and McIntosh, L. P. (2000) Hydrogen bonding and catalysis: a novel explanation for how a single amino acid substitution can change the pH optimum of a glycosidase, *J. Mol. Biol. 299*, 255−279.
49. Connelly, G. P., Withers, S. G., and McIntosh, L. P. (2000) Analysis of the dynamic properties of *Bacillus circulans* xylanase upon formation of a covalent glycosyl-enzyme intermediate, *Protein Sci. 9*, 512−524.
50. Törrönen, A., Harkki, A., and Rouvinen, J. (1994) Three-dimensional structure of endo-1,4-β-xylanase II from *Trichoderma reesei*: two conformational states in the active site, *EMBO J. 13*, 2493−2501.
51. McIntosh, L. P., Hand, G., Johnson, P. E., Joshi, M. D., Korner, M., Plesniak, L. A., Ziser, L., Wakarchuk, W. W., and Withers, S. G. (1996) The pK_a of the general acid/base carboxyl group of a glycosidase cycles during catalysis: a ^{13}C NMR study of *Bacillus circulans* xylanase, *Biochemistry 35*, 9958−9966.
52. Davoodi, J., Wakarchuk, W. W., Campbell, R. L., Carey, P. R., and Surewicz, W. K. (1995) Abnormally high pK_a of an active-site glutamic acid residue in *Bacillus circulans* xylanase. The role of electrostatic interactions, *Eur. J. Biochem. 232*, 839−843.
53. Koradi, R., Billeter, M., and Wüthrich, K. (1996) MOLMOL: a program for display and analysis of macromolecular structures, *J. Mol. Graphics 14*, 51−55.

BI049948M